2 um Raman laser based on CO_2-filled hollow-core silica fiber

Wang, Yazhou; Schiess, Olav T.S.; Correa, Rodrigo A.; Markos, Christos

Published in:
Fiber Lasers and Glass Photonics

Link to article, DOI:
10.1117/12.2624183

Publication date:
2022

Document Version
Publisher's PDF, also known as Version of record

PROCEEDINGS OF SPIE

SPIEDigitalLibrary.org/conference-proceedings-of-spie

2 μm Raman laser based on CO2-filled hollow-core silica fiber

Yazhou Wang, Olav T. S. Schiess, Rodrigo A. Correa, Christos Markos

Yazhou Wang, Olav T. S. Schiess, Rodrigo A. Correa, Christos Markos, "2 μm Raman laser based on CO2-filled hollow-core silica fiber," Proc. SPIE 12142, Fiber Lasers and Glass Photonics: Materials through Applications III, 121420O (25 May 2022); doi: 10.1117/12.2624183

SPIE.

Event: SPIE Photonics Europe, 2022, Strasbourg, France

2 um Raman laser based on CO_2-filled hollow-core silica fiber

Yazhou Wang*[a], Olav T. S. Schiess[a], Rodrigo A. Correa[b], and Christos Markos[a,c]
[a]DTU Fotonik, Technical University of Denmark, DK-2800 Kgs. Lyngby, Denmark; [b]CREOL, The College of Optics and Photonics, University of Central Florida, Orlando, FL-32816 USA;
[c]NORBLIS IVS, Virumgade 35D, DK-2830 Virum, Denmark.

ABSTRACT

Here, we present a high pulse energy Raman laser at 1946 nm wavelength pumped with a 1533 nm linearly polarized fiber laser, with ~92 μJ pulse energy, ~60 pm linewidth, 8 kHz repetition rate, and 7 ns pulse duration. The Raman laser is based on the stimulated Raman scattering (SRS) effect in an 8-meter carbon dioxide (CO_2) filled nested anti-resonant hollow-core fiber (ARHCF). The nested structure contributes to the significant reduction of the fiber loss caused by light leakage, surface scattering and bend, therefore allowing coiling the gas-filled ARHCF with a relatively small bend radius of just ~5 cm. When the pressure in the CO_2-filled ARHCF increases from 1 to 17 bar, the pulse energy first reaches the maximum pulse energy level of 16.3 μJ (corresponding to 28 % quantum efficiency) at only 1.2 bar, and then rapidly decreases due to the pressure-dependent overlap of the Raman laser line with the absorption band of CO_2 at 2 μm spectral range. The relative intensity noise (RIN) of the Raman laser reaches a minimum level (4%) when the pulse energy exceeds ~8 μJ. Due to the low amount of heat release during the SRS process, the laser has a good long-term stability without significant drift. Our results constitute a novel and promising technology towards high-energy 2 μm lasers.

Keywords: Raman laser, stimulated Raman scattering, anti-resonant hollow-core fiber, carbon dioxide

1. INTRODUCTION

Development of high energy and narrow linewidth fiber lasers at 2 μm has attracted significant research and commercial attention due to their use in different applications such as gas detection, optical parametric oscillator, laser surgery, etc. [1,2]. Thulium and holmium doped fibers based on population inversion are widely used for this purpose. However, the nonlinear effects (e.g., stimulated Brillouin/Raman scattering, nonlinear spectrum broadening), amplified spontaneous emission (ASE) and thermal damage are detrimental and unavoidable factors for the generation of narrow linewidth and high energy laser pulses [3,4]. The advent of gas-filled hollow-core fiber (HCF) Raman laser technology provides an alternative solution [5–7]. This laser technology relies on gas as the active gain medium, thus offering important advantages such as low nonlinearity and high damage threshold, while the relatively high threshold of SRS can effectively suppress the ASE frequency conversion [6,8–11]. Within the HCF family, emerging silica ARHCFs can overcome the high silica loss at ultraviolet and infrared regions by confining most of the laser beam within its hollow-core region with extremely low overlap with the surrounding glass structure [12–16]. Several reports have demonstrated 2 μm high-energy Raman laser generation by filling hydrogen (H_2) into the ARHCF, where the vibrational SRS was used for 2 μm laser conversion from a pump around 1 μm [5,6,17]. However, the use of high pressure H_2 adds an extra limitation of implementing these lasers in practical applications requiring portability. Furthermore, the use of H_2 introduces not only high permeability of silica over long time periods [18], but also a high amount of heat release because of the long vibrational Stokes shift coefficient (4155 cm-1), inducing thus a significant long term drift of the Raman laser [19]. The aforementioned challenges can be addressed by utilizing SRS through the rovibrational Q-branch of v1 band of the v1/2v2 Fermi dyad of CO_2 [20,21]. This is because its relatively small Stokes shift coefficient of 1385 cm-1 allows the direct generation of 2 μm laser from the 1.5 μm spectral range. Moreover, the remarkably narrow Raman gain linewidth (~ 300 MHz at 1 bar) formed by Dicke narrowing and collisional line-mixing effect is an important advantage for the development of ultra-narrow linewidth lasers [22]. Recently, a near-infrared (near-IR) frequency comb has been demonstrated based on cascaded SRS in a CO_2-filled ARHCF using a 1064 nm pump laser [23]. The cascaded SRS leads to the formation of a weak 3rd order Stoke line at 1911 nm driven by the 2nd Stoke at 1510 nm. Although the intensity of the 3rd order Stokes line is quite low due to the cascaded configuration and the long CO_2 molecule dephasing time relative to the pump pulse duration of ~450 ps, this work confirms that 2 μm laser can be achieved directly from a 1.5 μm pump. Here, we report our recent experiment result on a CO_2-filled ARHCF

Fiber Lasers and Glass Photonics: Materials through Applications III, edited by Maurizio Ferrari, Angela B. Seddon, Stefano Taccheo, Proc. of SPIE Vol. 12142, 121420O
 · 0277-786X · doi: 10.1117/12.2624183

Raman Stoke line at 1946 nm by using a 1533 nm fiber laser as pump [24]. A maximum pulse energy of up to 16.3 μJ (corresponding to 28 % quantum efficiency) is obtained with CO_2 pressure of only 1.2 bar.

2. EXPERIMENTAL METHOD AND RESULTS

Figure 1 presents the experimental setup. The pump laser consists of a directly modulated distributed feedback diode laser, followed by a three-stage amplification, to generate a pulse train with ~92 μJ energy, ~60 pm linewidth, 8 kHz repetition rate, and 7 ns pulse duration [25]. The pump is coupled into a 8-m long ARHCF with a coupling efficiency of ~80%. A half-wave plate (HWP) was used to optimize the pump polarization direction and therefore the SRS efficiency. The ARHCF is sealed by two gas cells that allows a maximum CO_2 pressure of 20 bar. The collimated output from the ARHCF passes through a CaF2 dispersive prism, to spatially separate the Raman laser from the residual pump, and to allow the simultaneous characterization of both lasers. A flip mirror is placed before the prism for laser's spectral characterization using an optical spectrometer (Spectro 320, Instrument Systems). The pulse profiles of the residual pump and Raman laser are respectively detected by a 5 GHz near-IR photodetector (DET08C/M, Thorlabs) and a 100 MHz mid-infrared photodetector (PDAVJ10, Thorlabs). The beam profiles are measured with a slit scanning beam profiler (BP109- IR2, Thorlabs).

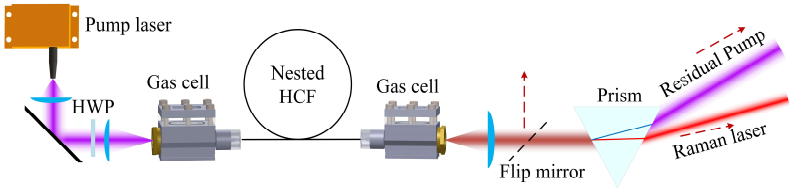

Figure 1. Experimental setup for the generation of the 1.94 μm Raman laser.

The ARHCF used, shown in Figure 2(a), has a nested structure, forming a hollow core region with diameter of ~37.6 μm [7]. The wall thickness and diameter are 406 nm and 22.2 μm for the outer capillaries, 621 nm and 6.04 μm for the nested (inner) capillaries, respectively. The nested structure contributes to the significant reduction of the fiber loss caused by light leakage, surface scattering and bend [26]. Our calculations indicated that, this structure enables a wide transmission in the near-IR range while having high loss in the mid-infrared (mid-IR), as shown in Figure 2(b). The relatively wide transmission window from 1.5 to 2 μm supports the 1st order Raman conversion, while significantly increases the threshold of higher order Stokes which cannot be reached by the 1st order Stokes with a pulse energy less than 20 μJ. As a result, the higher order Stokes are blocked, leading to the confinement of the full pulse energy only on the 1st order line. The losses at 1.53 μm and 1.95 um were found to be ~0.008 dB/m and ~0.35 dB/m, respectively.

A supercontinuum laser source (SuperK Extreme, NKT Photonics) was used to measure the transmission spectrum of the ARHCF. A ZBLAN fiber patch cable was used to couple the light into an optical spectrum analyzer (Spectro 320, Instrument Systems). Figure 2(c) shows the spectra of the supercontinuum laser before coupling into and after propagating through the ARHCF in ambient conditions, where they are normalized to facilitate comparison. The spectrum of propagating through the ARHCF exhibits a significant drop at ~850 nm, due to the resonance of the ARHCF. In the spectral region of ~1.1 to 2.4 μm, it can be seen that the difference between the two spectra increases at longer wavelengths, which could be attributed to the increase of the ARHCF loss.

We investigated the Raman laser power under different bend radii of 25 cm, 20 cm, 15 cm, and 10 cm. During this experiment the CO_2 pressure was maintained at atmospheric pressure. The results show that, the Raman pulse energy always remains at ~15.4 μJ, indicating that the fiber bend loss has a minor impact on the output power when the bend radii is larger than 10 cm. Figure 2(d) shows an image of the ARHCF, which is sealed inside a gas hose with 10 cm bend radius, used for the Raman laser generation. Given the risk of damaging the capillary structure of the ARHCF, bending the fiber with a radius of less than 10 cm was not implemented.

By properly setting the orientation of the HWP, the average Raman power was measured to be 122 mW at atmospheric pressure and maximum pump power that corresponds to 15.3 μJ pulse energy. According to the measured optical spectrum in Figure 3(a), the Raman laser has a center wavelength of 1946 nm. Given the ~60 pm pump linewidth, the Stokes shift coefficient of 1385 cm-1, and the ~300 MHz Raman gain linewidth, the Raman laser linewidth is estimated to be within the order of ~100 pm. This value exceeds the spectral resolution limit (0.2 nm) of our spectrometer and thus it cannot be accurately resolved.

It can be seen that the Raman spectrum has a high purity since the ASE is left on the pump wavelength region. In order to support this statement, we measured the ASE distributions of the output pump laser from the nested ARHCF,

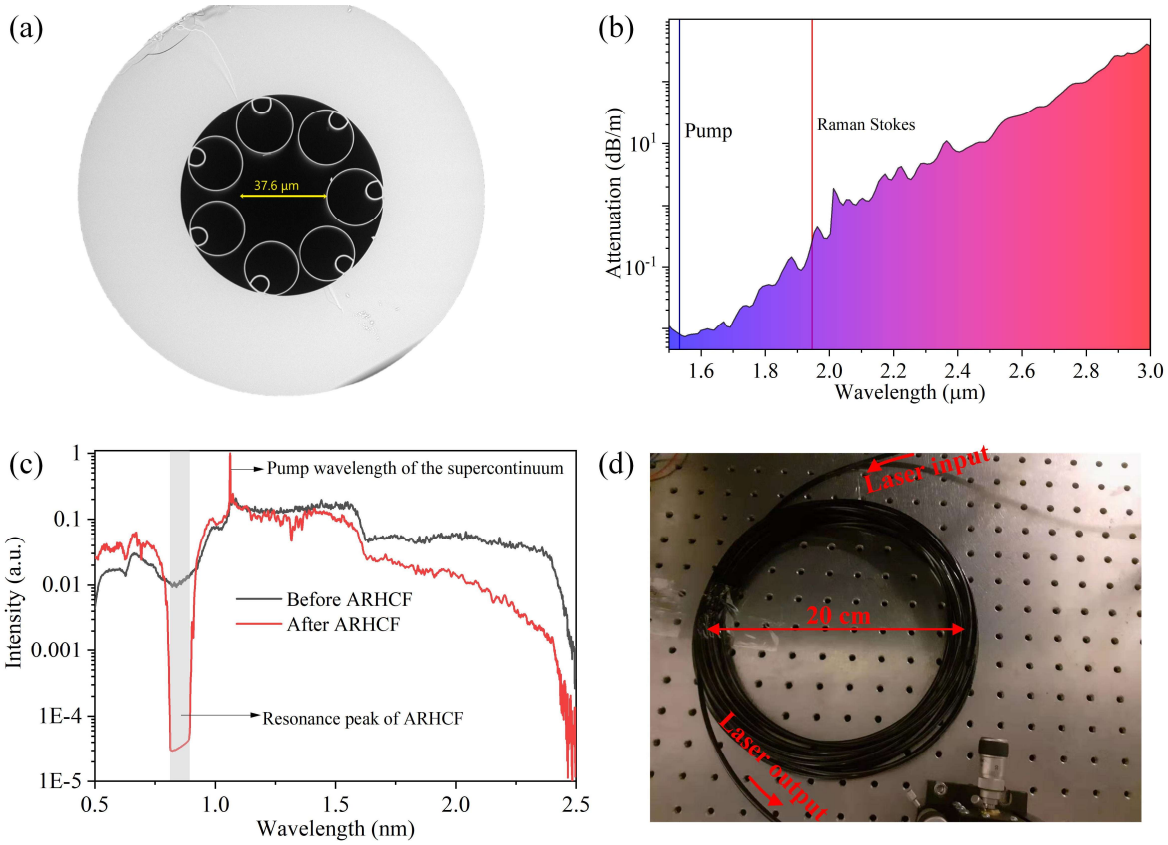

Figure 2. (a) Scanning electron microscopy image of the ARHCF. (b) Calculated fiber loss of the ARHCF using finite element method with COMSOL software (fiber bend loss is not included). (c) Spectra of a supercontinuum laser before coupling into and after propagating through the ARHCF filled with ambient air. (d) Experiment scene of the CO_2-filled ARHCF (inside gas hose) with a 10 cm bend radius.

filled with either pure CO_2 or Ar at atmospheric pressure. The former case corresponds to a Raman pulse energy of 15.4 μJ at 1.95 μm wavelength, while in the latter case the SRS process is prohibited. The spectrum was recorded by an optical spectrum analyzer (ANDO AQ6317B, AssetRelay) with a resolution of 0.01 nm. Figure 3(b) shows the measured spectra for both cases at the maximum pump power of 1.74 W. It can be seen that the spectrum in the case of pure CO_2 exhibits a much lower signal intensity while the pedestal profile is similar to the one of pure Ar. When the pump power decreases to 0.62 W, the SRS process diminishes, as a result the spectra in both cases show similar profiles, as shown in Figure 3(c). This effect clearly demonstrates that the SRS only occurs during laser's pulse part, and ASE is left in the pump wavelength region because of its low power level in time domain. The inset of Figure 3(a) shows the measured beam profiles of the Raman laser (left) and the residual pump (right). Both of them have a Gauss-like profile, indicating that the light mainly operates on the fundamental mode.

When the pressure in the CO_2-filled ARHCF increases over the range 1 to 17 bar, we found that the pulse energy quickly reaches the maximum value of 16.3 μJ (corresponding to 28 % quantum efficiency) at 1.2 bar, and then rapidly decreases, as shown in Figure 4(a). This tendency is different from other reported gas-filled ARHCF Raman lasers [25], where the pulse energy keeps increasing as the pressure increases, reaching eventually a saturation level [27]. The different trend in our experiment is attributed to the overlapping of the generated laser with the CO_2 absorption band, as indicated in Figure 4(a). The increase of the gas pressure inside the ARHCF fiber leads to the increase of the Raman gain bandwidth (due to the reduced gas molecule dephasing time) and consequently the laser linewidth [28], meanwhile it broadens the absorption linewidth of the CO_2 gas due to the enhanced molecule collisions. As a result, the overlap between the Raman laser line and CO_2 absorption line increases with the increase in the gas pressure. This was experimentally verified by investigating the direct CO_2 absorption of the Raman laser by passing the collimated laser beam through a gas chamber

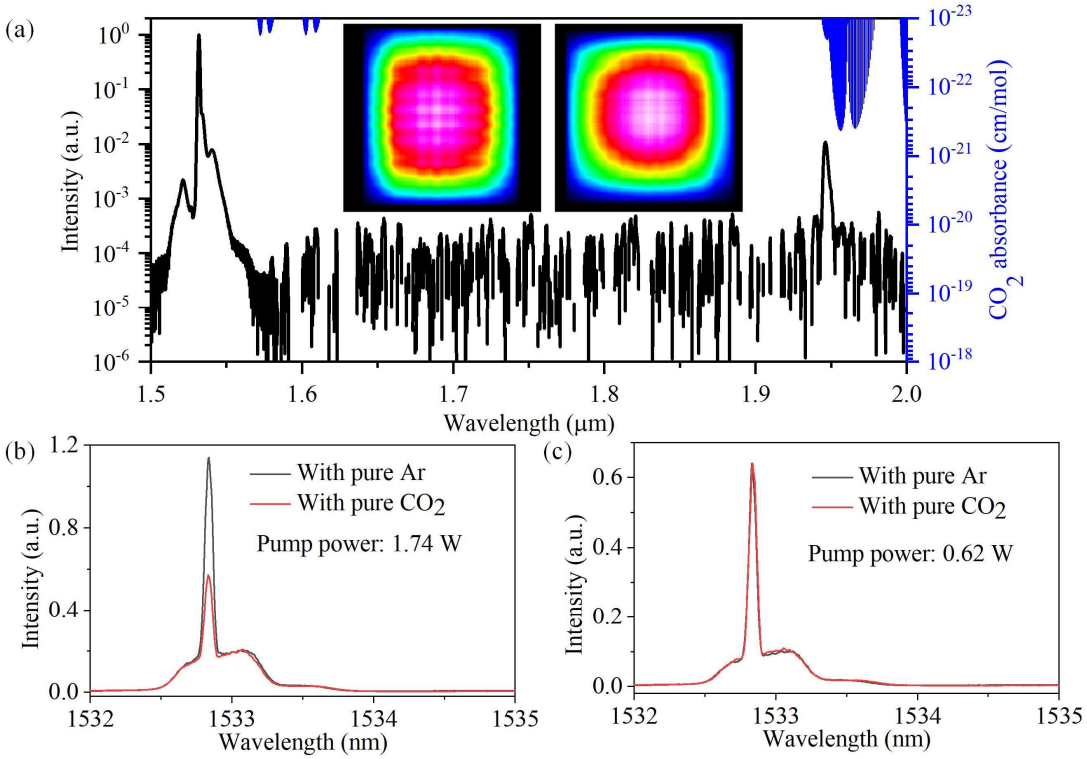

Figure 3. (a) The left axis shows the measured spectrum including both the residual pump and Raman laser. The right axis includes the absorption spectrum of CO_2 obtained from the high resolution transmission molecular absorption database [26]. Insets of (a) are measured beam profiles of the Raman laser (left) and the residual pump (right). (b) and (c) are comparison of measured spectrum of the output pump lasers from the nested ARHCF filled with either CO_2 or Ar at atmospheric pressure. The pump power is set to (b) a maximum level of 1.74 W and (c) 0.62 W, respectively, to generate a Raman pulse energy of 15.4 μJ and 0 μJ when the gas medium is CO_2.

filled with pure CO_2 at different pressures. The inner space of the gas chamber has a hollow cylindrical shape providing a 20 cm long optical path. Both ends of the chamber were sealed by two CaF_2 windows for gas filling. An infrared photodetector (PDAVJ10, Thorlabs) was used for recording the pulse peak intensity. Note that, although the peak intensity has a high pulse-to-pulse fluctuation due to quantum noise, its statistical behavior follows a stable distribution (see more details later), and therefore it can be used for measuring the CO_2 absorption. Figure 4(b) shows the effect of CO_2 absorption under different pressure (inside the chamber), where the Raman laser used for the absorption measurement was generated at a constant 10 bar pressure inside the ARHCF, in order to broaden the laser's linewidth and thus increase the overlap with CO_2 absorption. It can be seen that, when the CO_2 pressure inside the gas chamber increases from 1 to 15 bar, the peak intensity of our laser shows a corresponding decrease. When the CO_2 inside the chamber is replaced by pure argon, the peak intensity becomes independent on the pressure, further verifying the absorption effect of the CO_2. We also recorded the variation of the pulse peak intensity at atmospheric pressure, but at different CO_2 concentrations. The different concentrations were controlled using two different mass flow controllers with argon as diluting gas. Our measurements however did not reveal any observable difference on the peak intensity. This could be attributed to the relatively high pulse-to-pulse fluctuation of our Raman laser, the limited voltage resolution (12 bit) of our oscilloscope, as well as the weak absorption influence of CO_2 on the Raman laser at atmospheric pressure.

Figure 4(c) shows the impact of the pressure inside the ARHCF on the pulse profiles of both the Raman laser and the residual pump. Three Raman and corresponding residual pump pulse profiles at different pressure levels are recorded for comparison. Each pulse profile is an average of 10,000 measured pulses. To facilitate the comparison, the average power of these three Raman lasers are fixed to 4.4 mW by properly adjusting the pump power. The power coupling into the detector is precisely controlled by neutral density filters, to ensure that most of the laser pulses lies in the linear detection regime of the photodetector [19,29]. When the pressure increases from 2 to 10 bar, due to the suppression of the transient SRS

regime, the residual pump pulse duration on bottom of Figure 4(c) rapidly decreases from 5.3 ns to 3.0 ns, and a second peak gradually appears in the trailing edge region. The trailing edge of the Raman pulses (top of Figure 4(c)) exhibits an oscillation due to the 100 MHz bandwidth limitation of the mid-IR photodetector. It can be seen that the oscillation amplitude decreases with the increase of the pressure, indicating the increase of the Raman pulse duration. The decrease of the residual pump and the increase of the Raman pulse duration respectively at high pressure case are attributed to the associated decrease in molecular dephasing time, which is a crucial index for measuring the transition time from spontaneous Raman scattering to SRS state [30,31]. Another important observation is that the center (~ 6 – ~8 ns in Figure 4(c)-bottom) of the residual pump pulse profile at 10 bar is higher than the one at 5 bar. This is a sign that the Raman laser suffers from a high CO_2 absorption loss at highpressures, which is consistent with our deduction in Figure 4(b) and further verifies our initial assumption. Additionally, the Raman pulses in bottom of Figure 4(c) exhibit different delays in their leading edges. This phenomenon is attributed to the dependence of the Raman gain bandwidth and CO_2 absorption coefficient on CO_2 pressure. As the pressure of CO_2 increases, the former factor (bandwidth) will shorten the gas dephasing time and thus the delay, while the latter factor (absorption) will increase the threshold of SRS and the delay. As a result, the delay is a counteracted result of the two factors.

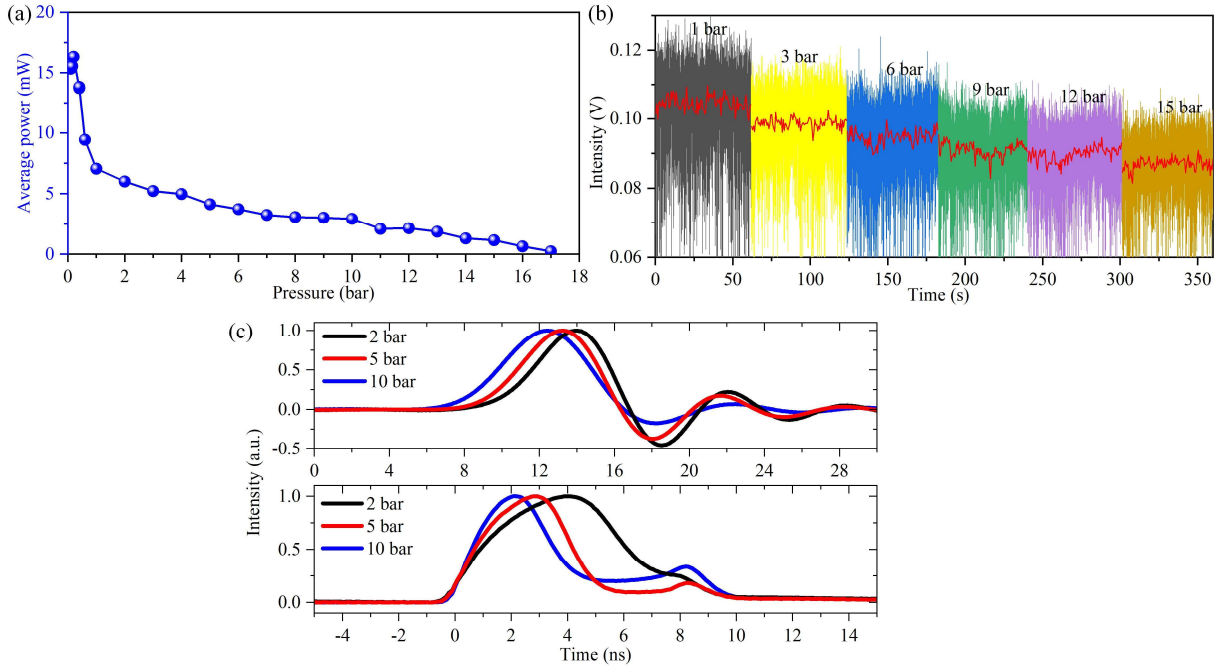

Figure 4. (a) Raman pulse energy versus the CO_2 pressure. (b) Measured pulse peak intensities of the Raman laser after passing through a 20 cm long gas chamber at different CO_2 pressures. (c) Average of 10,000 pulses at different pressures for Raman laser (top) and residual pump (bottom).

Since the SRS process is initiated by the random quantum noise, the Raman lasers have in general a relatively high pulse-to-pulse fluctuation [30]. Here we use RIN (defined as the ratio of the standard deviation to the mean value of pulse peak intensity) to describe the noise performance of our laser. Figure 5(a) shows the measured RIN of the Raman pulse peak intensity as a function of pulse energy. Each RIN value is counted based on 10,000 pulses. Initially, the RIN decreases with an increase of the average pulse energy, and then stabilizes at a minimum level of ~4% when the energy exceeds ~8 μJ. Insets of Figure 5(a) present the statistical distribution of the pulse peak intensity at two different average pulse energy levels. The distribution has a negative exponential distribution at a low energy of 0.125 μJ which reflects the behavior of quantum noise [30], and, due to the depletion of the pump power and the CO_2 molecules in the ground state during the SRS [31], it evolves to a Gaussian-like shape as the pulse energy increases. These effects are consistent with the conventional gas-chamber based Raman laser as well as our recent work using a H_2-filled ARHCF [22,30].

It is worth to emphasize that heat effect has been found to be a limiting factor to the performance of gas-filled ARHCF lasers [19]. A high amount of heat released during the SRS can significantly compromise the long-term stability of the laser [19]. In this work, due to the small photon energy difference between the pump and Raman Stokes, the maximum pulse

energy of 16.3 μJ is associated with a heat release of only 4.4 μJ, therefore the laser exhibits a good long-term stability without significant drift for more than 1 hour, as shown in Figure 5(b). Note that this measurement was recorded after 2 hours warming-up of the laser system, in order to stabilize the pump laser and the coupling efficiency from the pump to the ARHCF.

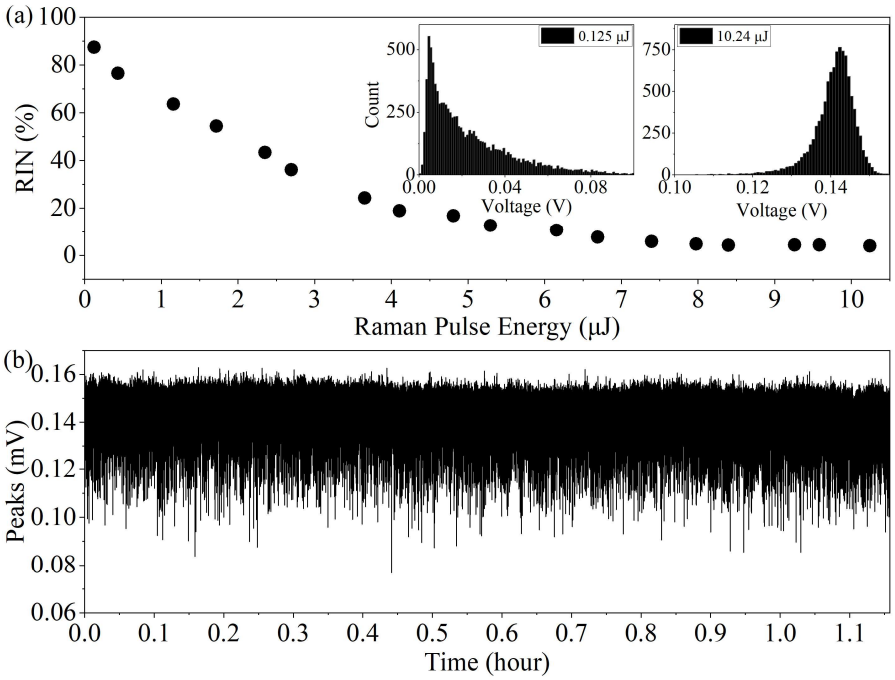

Figure 5. (a) RIN of the Raman laser measured at different pulse energies. Insets of (a) are histograms of peak intensity distributions of a 0.125 μJ (left) and a 10.2 μJ (right) pulse energy. (b) 200,000 Raman laser peaks measured at maximum Raman power over ~1.2 hour to show long-term stability.

3. CONCLUSION

In conclusion, we demonstrate that CO_2 can act as a Raman active medium for frequency conversion from ~1.5 μm to ~2 μm using the ARHCF technology. The maximum Raman pulse energy of 16.3 μJ was recorded at a gas pressure of only ~1.2 bar. The RIN of the Raman laser reaches a minimum level (4%) when the pulse energy exceeds ~8 μJ. Due to the low amount of heat release during the SRS, the laser has a good long-term stability without significant drift. Given the usual gain range of Er-doped fiber from ~1530 to ~1610 nm, the wavelength of the CO_2-filled fiber Raman laser could be easily extended to the range of ~1941 - ~2072 nm, therefore constituting a promising way towards 2 μm laser generation.

ACKNOWLEDGEMENTS

This work is supported by the LUNDBECK FONDEN (Grant NO. R346-2020-1924), Danmarks Frie Forskningsfond Hi-SPEC project (Grant No. 8022-00091B), VILLUM Fonden (Grant NO. 36063), Multi-BRAIN project funded by the Lundbeck Foundation (R276-2018-869), and US ARO (Grant No. W911NF-19-1-0426).

REFERENCES

[1] Scholle, K., Lamrini, S., Koopmann, P. and Fuhrberg, P., "2 μm laser sources and their possible applications," Front. Guid. Wave Opt. Optoelectron. (2010).

[2] Wang, Y., Feng, Y., Adamu, A. I., Dasa, M. K., Antonio-Lopez, J. E., Amezcua-Correa, R. and Markos, C., "Mid-infrared photoacoustic gas monitoring driven by a gas-filled hollow-core fiber laser," Sci. Rep. **11**(1), 3512 (2021).
[3] Jiang, H., Zhang, L. and Feng, Y., "Silica-based fiber Raman laser at >2.4 μm," Opt. Lett. **40**(14), 3249–3252 (2015).
[4] Tian, X., Zhao, X., Wang, M. and Wang, Z., "Suppression of stimulated Brillouin scattering in optical fibers by tilted fiber Bragg gratings," Opt. Lett. **45**(17), 4802–4805 (2020).
[5] Gladyshev, A. V, Kolyadin, A. N., Kosolapov, A. F., Yatsenko, Y. P., Pryamikov, A. D., Biryukov, A. S., Bufetov, I. A. and Dianov, E. M., "Efficient 1.9-μm Raman generation in a hydrogen-filled hollow-core fibre," Quantum Electron. **45**(9), 807–812 (2015).
[6] Wang, Z., Gu, B., Chen, Y., Li, Z. and Xi, X., "Demonstration of a 150-kW-peak-power, 2-GHz-linewidth, 1.9 μm fiber gas Raman source," Appl. Opt. **56**(27), 7657–7661 (2017).
[7] Adamu, A. I., Wang, Y., Habib, M. S., Dasa, M. K., Antonio-Lopez, J. E., Amezcua-Correa, R., Bang, O. and Markos, C., "Multi-wavelength high-energy gas-filled fiber Raman laser spanning from 1.53 μm to 2.4 μm," Opt. Lett. **46**(3), 452–455 (2021).
[8] Markos, C., Travers, J. C., Abdolvand, A., Eggleton, B. J. and Bang, O., "Hybrid photonic-crystal fiber," Rev. Mod. Phys. **89**(4), 45003 (2017).
[9] Benabid, F., Knight, J. C., Antonopoulos, G. and Russell, P. S. J., "Stimulated Raman scattering in hydrogen-filled hollow-core photonic crystal fiber," Science (80-.). **298**(5592), 399 LP – 402 (2002).
[10] Cao, L., Gao, S., Peng, Z., Wang, X., Wang, Y. and Wang, P., "High peak power 2.8 μm Raman laser in a methane-filled negative-curvature fiber," Opt. Express **26**(5), 5609–5615 (2018).
[11] Chen, Y., Wang, Z., Gu, B., Yu, F. and Lu, Q., "Achieving a 1.5 μm fiber gas Raman laser source with about 400 kW of peak power and a 6.3 GHz linewidth.", Opt. Lett. **41**(21), 5118–5121 (2016).
[12] Habib, M. S., Antonio-Lopez, J. E., Markos, C., Schülzgen, A. and Amezcua-Correa, R., "Single-mode, low loss hollow-core anti-resonant fiber designs," Opt. Express **27**(4), 3824 (2019).
[13] Klimczak, M., Dobrakowski, D., Ghosh, A.N., Stępniewski, G., Pysz, D., Huss, G., Sylvestre, T. and Buczyński, R., "Nested capillary anti-resonant silica fiber with mid-infrared transmission and low bending sensitivity at 4000 nm.", Opt. Lett. **44**(17), 4395–4398 (2019).
[14] Adamu, A. I., Habib, M. S., Petersen, C. R., Lopez, J. E. A., Zhou, B., Schülzgen, A., Bache, M., Amezcua-Correa, R., Bang, O. and Markos, C., "Deep-UV to mid-IR supercontinuum generation driven by mid-IR ultrashort pulses in a gas-filled hollow-core fiber," Sci. Rep. **9**(1), 4446 (2019).
[15] Selim Habib, M., Markos, C. and Amezcua-Correa, R., "Impact of cladding elements on the loss performance of hollow-core anti-resonant fibers," Opt. Express **29**(3), 3359–3374 (2021).
[16] Bache, M., Habib, M. S., Markos, C. and Lægsgaard, J., "Poor-man's model of hollow-core anti-resonant fibers," J. Opt. Soc. Am. B **36**(1), 69–80 (2019).
[17] Gladyshev, A. V, Kolyadin, A. N., Kosolapov, A. F., Yatsenko, Y. P., Pryamikov, A. D., Biriukov, A. S., Bufetov, I. A. and Dianov, E. M., "Low-threshold 1.9μm Raman generation in microstructured hydrogen-filled hollow-core revolver fibre with nested capillaries," Laser Phys. **27**(2), 25101 (2016).
[18] Kurita, N., Fukatsu, N., Otsuka, H. and Ohashi, T., "Measurements of hydrogen permeation through fused silica and borosilicate glass by electrochemical pumping using oxide protonic conductor," Solid State Ionics **146**(1), 101–111 (2002).
[19] Wang, Y., Adamu, A. I., Dasa, M. K., Antonio-Lopez, J. E., Habib, M. S., Amezcua-Correa, R., Bang, O. and Markos, C., "Noise performance and long-term stability of near- and mid-IR gas-filled fiber Raman lasers," J. Light. Technol. **39**(11), 3560–3567 (2021).
[20] Baran, J., Grofcsik, A. and Jones, W.J., "Motional narrowing in the $\nu_1/2\nu_2$ Fermi resonance diad of CO_2," Mol. Phys., **45**(6), 1291-1297 (1982).
[21] Lavorel, B., Millot, G., Saint-Loup, R., Berger, H., Bonamy, L., Bonamy, J. and Robert, D., "Study of collisional effects on band shapes of the $\nu_1/2\nu_2$ Fermi dyad in CO_2 gas with stimulated Raman spectroscopy. I. Rotational and vibrational relaxation in the $2\nu_2$ band," J. Chem. Phys. **93**(4), 2176–2184 (1990).
[22] Xiong, D., Bai, Y., Zuo, D. and Wang, X., "High-resolution continuous-wave coherent anti-Stokes Raman spectroscopy in a CO_2-filled hollow-core photonic crystal fiber," J. Raman Spectrosc. **52**(4), 857-864 (2021).
[23] "Intense stimulated Raman scattering in CO_2-filled hollow-core fibers.", Opt. Lett. **44**(21), 5318–5321 (2019).
[24] Wang, Y., Schiess, O. T. S., Amezcua-Correa, R. and Markos, C., "CO_2-based hollow-core fiber Raman laser with high-pulse energy at 1.95 μm," Opt. Lett. **46**(20), 5133–5136 (2021).
[25] Wang, Y., Dasa, M. K., Adamu, A. I., Antonio-Lopez, J. E., Habib, M. S., Amezcua-Correa, R., Bang, O. and

Markos, C., "High pulse energy and quantum efficiency mid-infrared gas Raman fiber laser targeting CO_2 absorption at 4.2 μm," Opt. Lett. **45**(7), 1938–1941 (2020).
[26] Poletti, F., "Nested antiresonant nodeless hollow core fiber," Opt. Express **22**(20), 23807–23828 (2014).
[27] Bischel, W. K. and Dyer, M. J., "Wavelength dependence of the absolute Raman gain coefficient for the Q(1) transition in H_2," J. Opt. Soc. Am. B **3**(5), 677–682 (1986).
[28] Bischel, W. K. and Dyer, M. J., "Temperature dependence of the Raman linewidth and line shift for the Q(1) and Q(0) transitions in normal and para-H_2," Phys. Rev. A **33**(5), 3113–3123 (1986).
[29] Adamu, A. I., Habib, M. S., Smith, C. R., Antonio Lopez, J. E., Uhd Jepsen, P., Amezcua-Correa, R., Bang, O. and Markos, C., "Noise and spectral stability of deep-UV gas-filled fiber-based supercontinuum sources driven by ultrafast mid-IR pulses," Sci. Rep. **10**(1), 4912 (2020).
[30] Raymer, M. G. and Walmsley, I. A., "III the quantum coherence properties of stimulated Raman scattering," E. B. T.-P. in O. Wolf, Ed., Elsevier, 181–270 (1990).
[31] Walmsley, I. A., Raymer, M. G., Sizer, T., Duling, I. N. and Kafka, J. D., "Stabilization of stokes pulse energies in the nonlinear regime of stimulated Raman scattering," Opt. Commun. **53**(2), 137–140 (1985).